AWARD NUMBER: W81XWH-12-1-0412

TITLE: Proteomic Analysis to Identify Functional Molecules in Drug Resistance Caused by E-Cadherin Knockdown in 3D-Cultured Colorectal Cancer Models

PRINCIPAL INVESTIGATOR: Xiaoshan Yue

CONTRACTING ORGANIZATION: University of Notre Dame Du Lac
                                             Notre Dame, IN 46556

REPORT DATE: September 2014

TYPE OF REPORT: Annual Report

PREPARED FOR: U.S. Army Medical Research and Materiel Command
                         Fort Detrick, Maryland 21702-5012

DISTRIBUTION STATEMENT: Approved for Public Release;
                                        Distribution Unlimited

The views, opinions and/or findings contained in this report are those of the author(s) and should not be construed as an official Department of the Army position, policy or decision unless so designated by other documentation.

REPORT DOCUMENTATION PAGE

Form Approved
OMB No. 0704-0188

Public reporting burden for this collection of information is estimated to average 1 hour per response, including the time for reviewing instructions, searching existing data sources, gathering and maintaining the data needed, and completing and reviewing this collection of information. Send comments regarding this burden estimate or any other aspect of this collection of information, including suggestions for reducing this burden to Department of Defense, Washington Headquarters Services, Directorate for Information Operations and Reports (0704-0188), 1215 Jefferson Davis Highway, Suite 1204, Arlington, VA 22202-4302. Respondents should be aware that notwithstanding any other provision of law, no person shall be subject to any penalty for failing to comply with a collection of information if it does not display a currently valid OMB control number. **PLEASE DO NOT RETURN YOUR FORM TO THE ABOVE ADDRESS.**

1. REPORT DATE	2. REPORT TYPE	3. DATES COVERED
September 2014	Annual Report	1 Sep 2013 – 31 Aug 2014

4. TITLE AND SUBTITLE
Proteomic Analysis to Identify Functional Molecules in Drug Resistance Caused by E-Cadherin Knockdown in 3D-Cultured Colorectal Cancer Models

5a. CONTRACT NUMBER

5b. GRANT NUMBER
W81XWH-12-1-0412

5c. PROGRAM ELEMENT NUMBER

6. AUTHOR(S)
Xiaoshan Yue, Amanda B. Hummon

5d. PROJECT NUMBER

5e. TASK NUMBER

5f. WORK UNIT NUMBER

E-Mail: xyue@nd.edu; ahummon@nd.edu

7. PERFORMING ORGANIZATION NAME(S) AND ADDRESS(ES)
University of Notre Dame Du Lac
Notre Dame, Indiana 465556

8. PERFORMING ORGANIZATION REPORT NUMBER

9. SPONSORING / MONITORING AGENCY NAME(S) AND ADDRESS(ES)

U.S. Army Medical Research and Materiel Command
Fort Detrick, Maryland 21702-5012

10. SPONSOR/MONITOR'S ACRONYM(S)

11. SPONSOR/MONITOR'S REPORT NUMBER(S)

12. DISTRIBUTION / AVAILABILITY STATEMENT

Approved for Public Release; Distribution Unlimited

13. SUPPLEMENTARY NOTES

14. ABSTRACT

In the second year of research, we successfully optimized the SILAC methods and phosphoproteomic analysis methods. The optimized method has increased the phosphopeptide identification for 2 folds. We also optimized the system for testing drug effects. Four different drugs including irinotecan, oxaliplatin, 5-FU, and gefitinib were tested with CDH1 knock down cells for drug resistance effects. Cells with down regulated CDH1 levels show resistance to all drugs at high concentration except 5-FU. The mass spectrum data for drug resistance pathways are under collection and investigation. We also analyzed the proteomic and phosphoproteomic differences between 2D and 3D cultured cells.

In conclusion, during the second year, we accomplished most of the work we proposed in our original proposal, and finished the tasks that got delayed during the first year. The second year's research is a good extension of the first year research, and provided us the foundation for our future work.

15. SUBJECT TERMS
CDH1 knock-down, EMT, metastasis, drug resistance

16. SECURITY CLASSIFICATION OF:			17. LIMITATION OF ABSTRACT	18. NUMBER OF PAGES	19a. NAME OF RESPONSIBLE PERSON USAMRMC
a. REPORT	**b. ABSTRACT**	**c. THIS PAGE**	Unclassified	28	**19b. TELEPHONE NUMBER** (include area code)
Unclassified	Unclassified	Unclassified			

Standard Form 298 (Rev. 8-98)
Prescribed by ANSI Std. Z39.18

Table of Contents

INTRODUCTION

Metastasis is one of the biggest problems in cancer therapy. E-cadherin (CDH1) is known to be involved in epithelial-mesenchymal transition (EMT) process, thus playing an important role during the tumor metastatic progression [1-3]. It is reported that losing CDH1 expression in conjunction with EMT might contribute to the development of multidrug resistance (MDR) to chemotherapy [4-6]. Thus, understanding the CDH1 down-regulation mediated EMT and its relationship with MDR will have great benefit for improving chemotherapy efficiency. Most of the present *in vitro* research analyzing the functions of CDH1 and its involvement in mediating metastasis have been carried out in 2D cultured cell lines. However, it has been reported that cells in 2D-culture systems have different gene expression patterns than *in vivo* cells [7-11]. By comparison, the 3D culture systems provide more accurate molecular pictures of human disease. The establishment of 3D-culture systems will be a better way to mimic the tissue samples and provide us with more information that recapitulates human tissues.

In this study, we aim to establish a 3D model that can simulate the *in vivo* cancer models and can be induced to down regulate its CDH1 expression when stimulated, and thus can be used for simulation of EMT processes. We selected CDH1 as a target for manipulation because its expression is known to cause pronounced chemical and phenotypic changes in epithelial cells. The CDH1 knock down needs to be inducible as expression of CDH1 is essential during formation of the 3D structures and the CDH1 will be knocked down after the 3D structures are fully formed. We hypothesize that by reducing the expression of CDH1 in colorectal cancer cell lines cultured in 3D-structures, the colorectal cancer cells will display EMT characteristics and gain drug-resistance compared to CDH1 (+) colorectal cancer cells. We hypothesize that CDH1 reduction will induce changes in downstream pathways, including proteins in pathways of cell survival (PI3K, GSK3b, EGFR) apoptosis (caspases family proteins, Bcl-2 family proteins), and cell migration (Rho family proteins like Cdc42, Rac1, RhoA, WASP family proteins, and PAR/aPKC complexes). *Our research will be the first to connect EMT to drug resistance in 3D-culture systems.*

During the first year of this research, we put our effort mainly into establishing and optimizing the inducible CDH1 knock down model with 3D culturing system, and evaluating its characteristics and performance. During the second year of this research, we put our effort mainly into establishing and optimizing the methodology for proteomic and phosphoproteomic analysis, and started to collect data for evaluating the functions of CDH1 for drug resistance with mass spectrometer. These data will be analyzed for changes in the signal transduction pathways mentioned above.
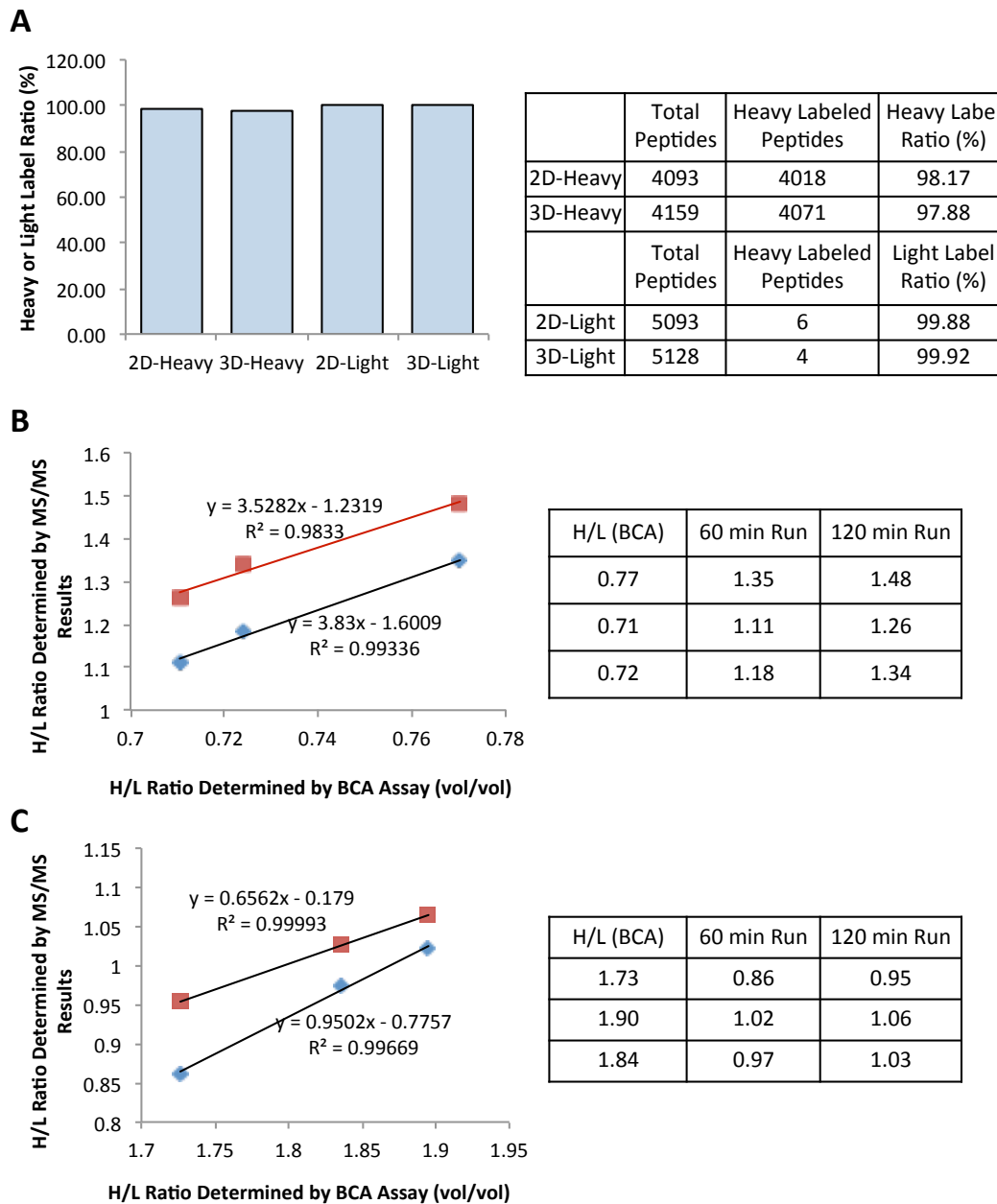
KEY WORDS

CDH1 knock-down, EMT, metastasis, drug resistance

ACCOMPLISHMENTS

1. (Task 2a) Establish the SILAC method. (7/1/2013-8/30/2013)

In our proposed research, we will perform quantitative experiments to study the molecular changes of 3D structures in response to CDH1-KD induced drug resistance. We will use the Stable Isotope Labeling of Amino Acids in Cell Culture (SILAC) strategy to label 3D structures under different conditions, and then mix the samples together and perform LC-MS/MS analysis. To prepare for the quantitative analysis, we first analyzed the labeling efficiency of the SILAC method. SILAC labels were checked both in 2D and 3D culturing systems. The results show that in both 2D and 3D culturing systems, for the cells cultured in media supplemented with heavy amino acids, around 98% of peptides were labeled with heavy amino acids. For the cells cultured in media supplemented with light amino acids, more than 99.8% of the peptides have light amino acids, and the presence of heavy amino acids is less than 0.2% (**Figure 1A**). The protein amounts in each sample were determined by BCA assay. However, because the BCA assay can sometimes generate some error, to ensure that in the real experiments the light and heavy samples can be mixed with exactly a 1:1 ratio, a pre-experiment was performed to determine the actual heavy-to-light mixing ratio (vol/vol). The heavy-labeled 3D structures and light-labeled 2D layers were mixed with different volume ratios to make a 1:1 total protein ratio determined by BCA assay (**Figure 1B**). Six samples were generated with different vol/vol ratios and tested with LC-MS/MS with 60 min run (blue line in **Figure 1B**) and 120 min run (red line in **Figure 1B**). The heavy-to-light ratio determined by LC-MS/MS showed a linear correlation to the vol/vol ratios determined by BCA assay. The light-labeled 3D structures and heavy-labeled 2D structures were tested with the same strategy and showed similar results (**Figure 1C**). From these linear correlations we determined the actual vol/vol ratio to verify that the peptide heavy-to-light ratio was 1:1 for both 60 min and 120 min runs. We will use the average of these two numbers to make the heavy and light sample mixtures.
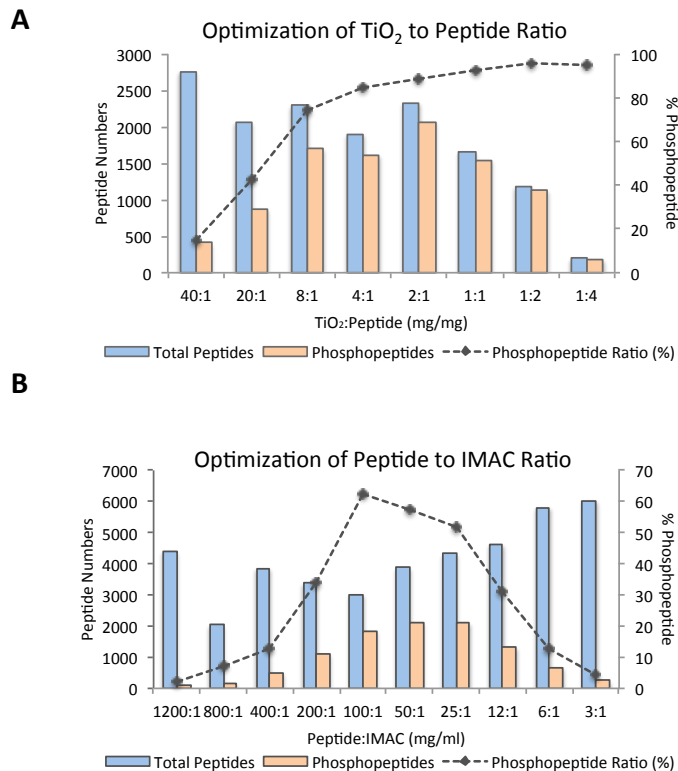
Figure 1

A

	Total Peptides	Heavy Labeled Peptides	Heavy Label Ratio (%)
2D-Heavy	4093	4018	98.17
3D-Heavy	4159	4071	97.88
	Total Peptides	Heavy Labeled Peptides	Light Label Ratio (%)
2D-Light	5093	6	99.88
3D-Light	5128	4	99.92

B

y = 3.5282x - 1.2319
R^2 = 0.9833

y = 3.83x - 1.6009
R^2 = 0.99336

H/L (BCA)	60 min Run	120 min Run
0.77	1.35	1.48
0.71	1.11	1.26
0.72	1.18	1.34

C

y = 0.6562x - 0.179
R^2 = 0.99993

y = 0.9502x - 0.7757
R^2 = 0.99669

H/L (BCA)	60 min Run	120 min Run
1.73	0.86	0.95
1.90	1.02	1.06
1.84	0.97	1.03

Figure 1. SILAC labeling efficiency. (A) SILAC heavy and light amino acid label efficiencies are shown in bar graph. (B, C) Validation of the ratio (vol/vol) to mix heavy and light samples to make 1:1 SILAC mixtures. (B) is for the mixture of heavy-labeled 3D structures and light-labeled 2D layers, and (C) is for the mixture of light-labeled 3D structures and heavy-labeled 2D layers.

2. (Task 2a - Extension) Optimizing phosphoproteomic methods for phosphoprotein quantification. (9/1/2013-1/31/2014)

Phosphorylation and dephosphorylation of key cellular factors and the deregulation of kinase signaling pathways are commonly associated with various cancers. Among the many biochemical mechanisms involved in cellular signaling, protein phosphorylation is one of the most common control mechanisms to regulate a variety of biological processes, including cell proliferation, migration, DNA reparation, and apoptosis. Over the past decades, great efforts were made to estimate the phosphorylation level of signaling pathways in different types of cancers. Phosphorylation events were reported in lung cancer, breast cancer, colorectal cancer, pancreatic cancer, and prostate cancer. We published a manuscript in *Journal of Proteome Research* in the first year of the project introducing a new phosphoproteomic enrichment workflow that works better than the gold standard. We are further improving that method with the following study.

In order to make it possible to identify as many phosphoproteins and phosphosites as possible, we also optimized the methods for mass spectrometric-based phosphoproteomic studies. In our experiments, we compared two materials including IMAC and TiO_2 that are widely used to enrich phosphopeptides from the peptide mixtures for phosphoproteomic studies.

We first optimized the TiO_2 or IMAC bead to peptide ratios to achieve the best performance of the beads (**Figure 2**). The results show that TiO_2 beads perform best with the TiO_2 to peptide ratio ranging from 2:1 to 8:1, which can achieve more than 80% phosphopeptide enrichment efficiency without losing total phosphopeptide identifications (**Figure 2A**). The IMAC beads show the best performance when the peptide to IMAC ratio is 100:1, which shows the highest enrichment efficiency of more than 60% (**Figure 2B**).
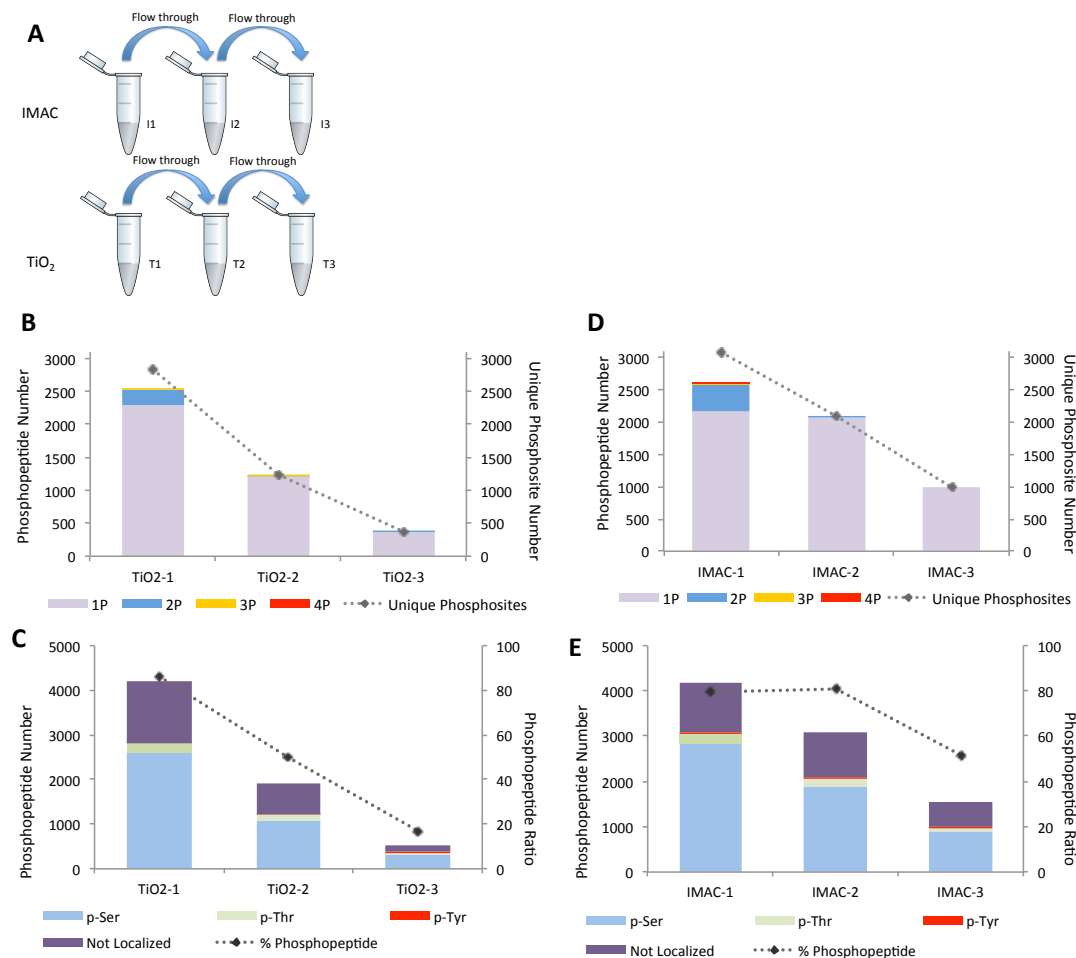
Figure 2

Fig 2. Optimization of the peptide to bead ratio for phosphopeptide enrichment from whole cell lysate. (A) Optimization of TiO_2 to peptide ratio. (B). Optimization of peptide to IMAC ratio. Identified total peptide numbers with different TiO_2-to-peptide ratios (μg:μg) or peptide-to-IMAC ratios (μg:μl) are shown in the bar graph. Percentages of identified phosphopeptides with each condition are shown with the dashed line.

With the optimized material to peptide ratios, we performed direct enrichment of phosphopeptides with IMAC or TiO_2 beads from whole cell lysates. As starting material, 3 mg of MCF-10A cell lysate were used for phosphopeptide enrichment. According to the optimized material to peptide ratios, we added 30 μl of the IMAC or 6 mg of TiO_2 bead slurry to the peptide mixture to perform phosphopeptide enrichment. The results showed that a total of 4811 peptides were identified with the first round of TiO2 enrichment (TiO_2-1) and among which 3918 were phosphopeptides, with a phosphopeptide enrichment ratio of 81.4% (**Figure 3B&C**). A total of 4661 peptides were identified with the first round of IMAC enrichment (IMAC-1), and among these peptides, 3699 were phosphopeptides, with a phosphopeptide enrichment ratio of 79.4% (**Figure 3D&E**). PhosphoRS was used to evaluate the accuracy of phosphosites

localization [12]. As reported previously, phosphopeptides with PhosphoRS score $\geq$ 99% are considered to have confident phosphosite localization [12]. We only counted phosphopeptides with confident localization for mono- or multi-phosphopeptide identification, as well as for calculating total number of phosphosites identified in all species. TiO_2-1 enrichment generated 2631 phosphopeptides with confident localization information, among which 2382 were mono-phosphopeptides, while 249 were multi-phosphopeptides (**Figure 3B&C**). IMAC-1 enrichment generated 2608 phosphopeptides with confident localization information, among which 2166 were mono-phosphopeptides, and 442 were multi-phosphopeptides (**Figure 3D&E**).
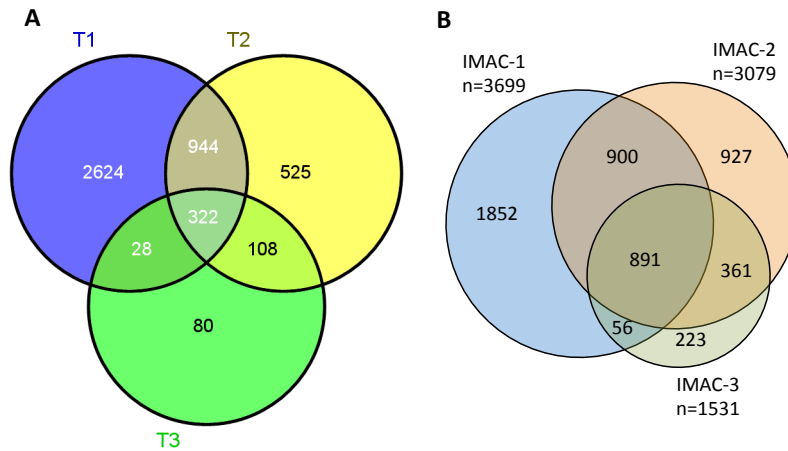
Figure 3

Fig 3. Distribution of phosphopeptides identified by multi-step TiO_2 or IMAC enrichment. (A) Experiment workflow for multiple rounds of enrichment. (B) Numbers of identified phosphopeptides in the first, second, and third round of TiO_2 enrichment (phosphoRS score $\geq$ 99%) with 1, 2, 3, or 4 phosphate groups are shown in the bar graph with light purple, blue, yellow and red colors. Unique

phosphosite numbers are calculated from phosphopeptides with phosphoRS score $\geq$ 99% and are shown with the dashed line. (C) Numbers of identified phosphopeptides in the first, second, and third round of TiO_2 enrichment with phospho-serine (blue), phospho-threonine (green), or phospho-tyrosine (red) sites, and those without confident localization (phosphoRS score < 99%, dark purple) are shown in the bar graph. The percentages of identified phosphopeptides from the total identified peptides in each round of IMAC enrichment are shown with the dashed line. (D) Numbers of identified phosphopeptides in the first, second, and third round of IMAC enrichment (phosphoRS score $\geq$ 99%) with 1, 2, 3, or 4 phosphate groups are shown in the bar graph with light purple, blue, yellow and red colors. Unique phosphosite numbers are calculated from phosphopeptides with phosphoRS score $\geq$ 99% and are shown with the dashed line. (E) Numbers of identified phosphopeptides in the first, second, and third round of IMAC enrichment with phospho-serine (blue), phospho-threonine (green), or phospho-tyrosine (red) sites, and those without confident localization (phosphoRS score < 99%, dark purple) are shown in the bar graph. The percentages of identified phosphopeptides from the total identified peptides in each round of IMAC enrichment are shown with the dashed line.

To evaluate how complete a single enrichment would be at extracting phosphopeptides from the whole cell lysate, we then carried out a second round of enrichment from the flow-through of the first round of enrichment. We repeated the process for a third round, with enrichment from the flow-through of the second round of enrichment. In the second round of TiO_2 enrichment, 1899 total phosphopeptides were identified. Of these, 1266 phosphopeptides were also identified with the first round of TiO_2 enrichment, while 525 phosphopeptides were unique to the second round enrichment. With the third round of TiO_2 enrichment, a total number of 538 phosphopeptides were identified, among which 350 phosphopeptides had been identified with the first round of TiO_2 enrichment and 430 phosphopeptides overlapped with the second round of TiO_2 enrichment. Only an additional 80 unique phosphopeptides were detected with the third round of TiO_2 enrichment (**Figure 4A**). In the second round of IMAC enrichment, 3079 total phosphopeptides were identified. Of these, 1791 phosphopeptides were also identified with the first round of IMAC enrichment, while 1288 phosphopeptides were unique to the second round phosphopeptides. With the third round of IMAC enrichment, a total number of 1531 phosphopeptides were identified, among which 947 phosphopeptides had been identified with the first round of IMAC enrichment and 1252 phosphopeptides overlapped with the second round of IMAC enrichment. Only an additional 223 unique phosphopeptides were detected with the third

round of IMAC enrichment (**Figure 4B**). All the above results indicate that three cycles of TiO_2 or IMAC enrichment would be enough to enrich most of the phosphopeptides from the whole cell lysates.
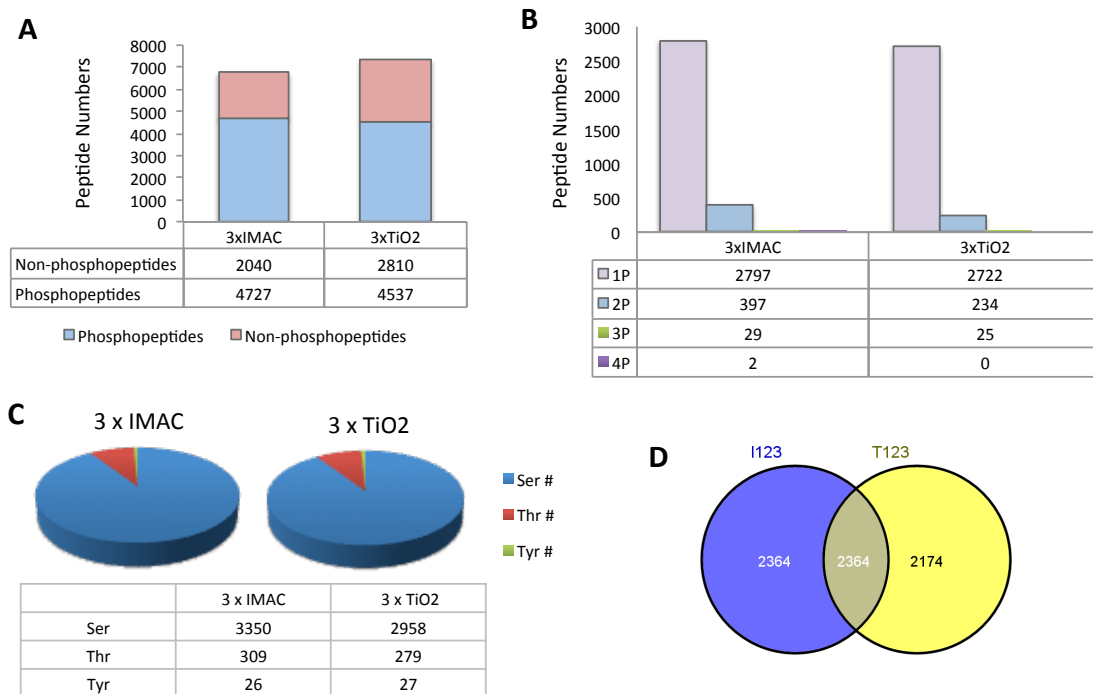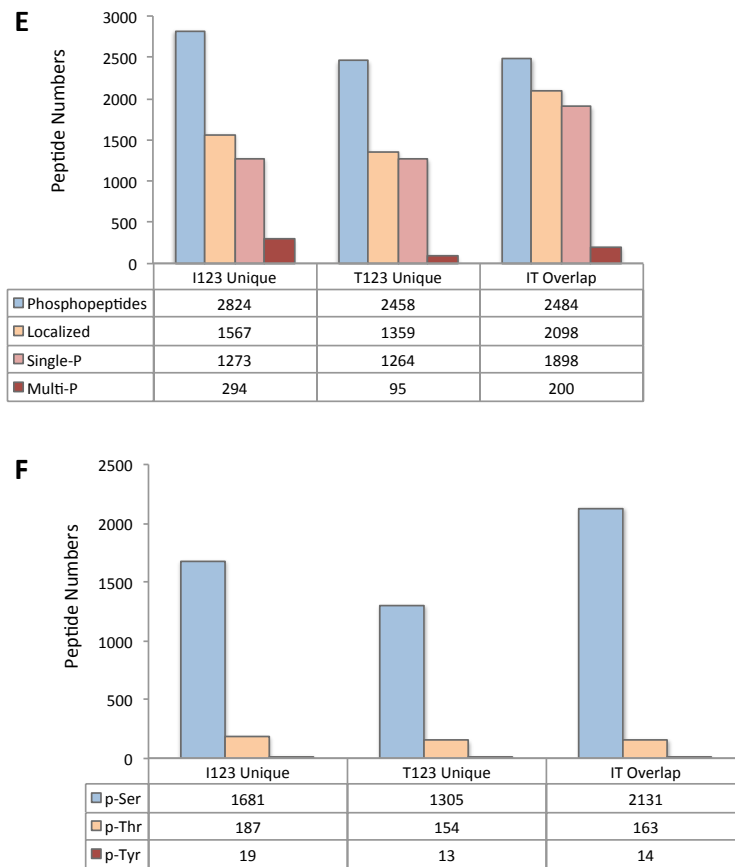
Figure 4

Fig 4. Venn diagram of phosphopeptides identified by multi-step TiO_2 or IMAC enrichment. (A) Overlaps of the nonredundant phosphopeptides identified in each round of TiO_2 enrichment are shown in the Venn diagram. (D) Overlaps of the nonredundant phosphopeptides identified in each round of IMAC enrichment are shown in the Venn diagram.

We next compared the differences of phosphopeptides that are enriched with the multiple rounds of TiO_2 or IMAC. A total number of 4727 unique phosphopeptides were identified with 3 rounds of IMAC enrichment, while a total number of 4537 unique phosphopeptides were identified with 3 rounds of TiO_2 enrichment, showing that both IMAC and TiO_2 have the equivalent ability to enrich phosphopeptides from whole cell lysate (**Figure 5A**). IMAC enriched 2793 mono-phosphopeptides and 428 multi-phosphopeptides, while TiO_2 enriched 2722 mono-phosphopeptides and 259 multi-phosphopeptides, indicating that IMAC is more efficient for enriching multi-phosphopeptides. The distribution of phosphor-Ser, phosphor-Thr and phosphor-Tyr with IMAC or TiO_2 enrichment is shown in **Figure 5C**, and does not show much difference with these two different enrichment methods. However, the overlap between phosphopeptides identified with IMAC or TiO_2 shows only about 1/3 of the phosphopeptides were identified with both IMAC and TiO_2 enrichment (**Figure 5D**). Among the overall identified phosphopeptides, 2364 were unique to IMAC enrichment, 2174 were unique to TiO_2 enrichment, and 2364 were identified with both methods

(**Figure 5D**). In order to further investigate how the IMAC enrichment is different from TiO$_2$ enrichment, we divided the overall identified phosphopeptides into 3 subsets, the first subset consists of phosphopeptides that are uniquely identified by IMAC enrichment, the second subset contains phosphopeptides that are uniquely identified by TiO$_2$ enrichment, and the third subset is phosphopeptides that are identified both with IMAC and TiO$_2$ enrichment. *The results clearly show that the phosphopeptides that are uniquely identified with IMAC enrichment contain 3 times as many as multi-phosphopeptide compared with those that are uniquely identified with TiO$_2$* (**Figure 5E**). In comparison, the percentage of phosphor-Ser, phosphor-Thr, and phosphor-Tyr does not show much difference among these 3 parts (**Figure 5F**). *This result is significant as multi-phosphorylated peptides are biologically important but obtain hard to detect and characterize. With this approach, we have determined an optimized approach to identify multi-phosphorylated peptides from complex biological samples.*
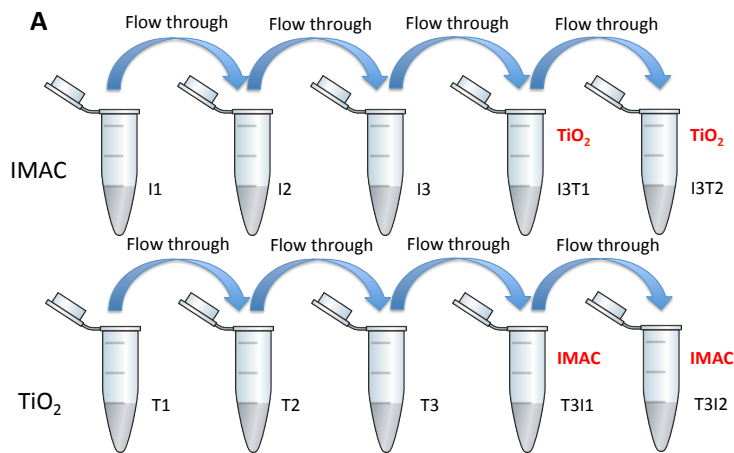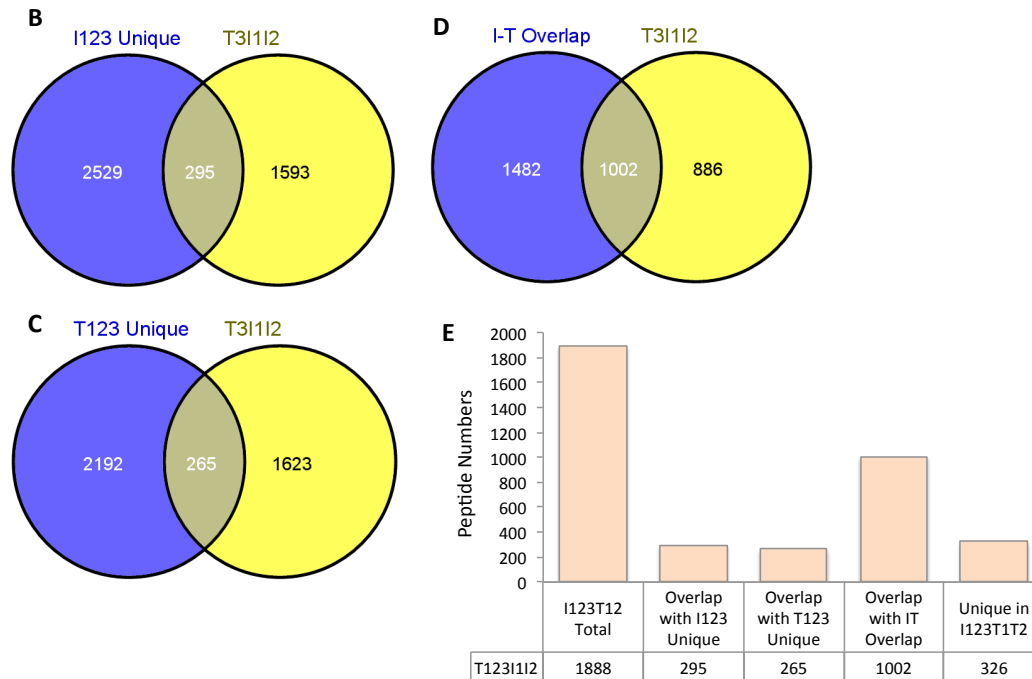
Figure 5

A

	3xIMAC	3xTiO2
Non-phosphopeptides	2040	2810
Phosphopeptides	4727	4537

■Phosphopeptides ■Non-phosphopeptides

B

	3xIMAC	3xTiO2
□1P	2797	2722
□2P	397	234
□3P	29	25
■4P	2	0

C

3 x IMAC   3 x TiO2

■Ser #
■Thr #
■Tyr #

	3 x IMAC	3 x TiO2
Ser	3350	2958
Thr	309	279
Tyr	26	27

D

I123   T123

2364   2364   2174

Figure 5

E

	I123 Unique	T123 Unique	IT Overlap
▢ Phosphopeptides	2824	2458	2484
▢ Localized	1567	1359	2098
▢ Single-P	1273	1264	1898
▢ Multi-P	294	95	200

F

	I123 Unique	T123 Unique	IT Overlap
▢ p-Ser	1681	1305	2131
▢ p-Thr	187	154	163
▢ p-Tyr	19	13	14

Fig 5. Comparison between TiO_2 and IMAC enriched phosphopeptides. (A) Distribution of non-phosphopeptides and phosphopeptides identified with TiO_2 or IMAC enrichment. (B) Distribution of phosphopeptides with 1, 2, 3, or 4 phosphate groups identified with TiO_2 or IMAC enrichment. (C) Distribution of phosphopeptides with phospho-serine, phospho-threonine, or phospho-tyrosine sites identified with TiO_2 or IMAC enrichment. (D) Overlaps of the nonredundant phosphopeptides identified with TiO_2 or IMAC enrichment are shown in the Venn diagram. (E) Distribution of single or multi-phosphopeptides that are identified as IMAC unique, TiO_2 unique, or with both enrichment methods. (F) Distribution of phosphopeptides with phospho-serine, phospho-threonine, or phospho-tyrosine sites that are identified as IMAC unique, TiO_2 unique, or with both enrichment methods.

We next evaluated whether the differences of phosphopeptides enriched by IMAC or TiO_2 result from the enrichment step, or from the elusion step. We used 2 rounds of

TiO$_2$ to further enrich phosphopeptides from the flow-through of 3 rounds of IMAC enrichment, and we used 2 rounds of IMAC to further enrich phosphopeptides from the flow-through of 3 rounds of TiO$_2$ enrichment (**Figure 6A**). The results show that with further TiO$_2$ enrichment from the flow-through of IMAC enrichment, the identified phosphopeptides doesn't show much overlap with those that are identified with TiO$_2$ enrichment from the whole cell lysate (**Figure 6B-E**), *indicating that the loss of phosphopeptide identification is not due to the incomplete enrichment from the cell lysate, but is due to the incomplete elution from IMAC or TiO$_2$ materials.*

Figure 6

Figure 6

Fig 6. Distribution of phosphopeptides identified by multi-step TiO$_2$ following multi-step IMAC enrichment. (A) Experiment workflow for multiple rounds of enrichment. (B-D) Overlap of TiO$_2$ enriched phosphopeptides from IMAC flow-through with phosphopeptides in IMAC unique, TiO$_2$ unique, or IMAC-TiO$_2$ overlap parts. **(E)** Distribution of phosphopeptides identified in each round of TiO$_2$ or IMAC enrichment.

To evaluate the contribution of each round of enrichment to the total unique phosphopeptide identification, for each round of enrichment, the total number of identified phosphopeptides and the number of unique phosphopeptides are summarized in **Figure 7A**. The results show that the first round of IMAC or TiO$_2$ enrichment gave the highest number of both total phosphopeptide and unique phosphopeptide identification, while the identification decreases for the second and third round of enrichment with the same material (**Figure 7A**). However, by switching the enrichment material to the other media, the identification numbers increased again (**Figure 7A**). By integrating IMAC with TiO$_2$ enrichment, the total number of identified phosphopeptides has reached 8747 with just 2 days of workload. The contribution of each round of enrichment for identification of unique phosphopeptides is summarized in **Figure 7B**.

Figure 7

A

B

Fig 7. Distribution of phosphopeptides identified in each round of TiO_2 or IMAC enrichment. (A) Distribution of total phosphopeptides (blue) and unique phosphopeptides (pink) identified in each round of TiO_2 or IMAC enrichment. (B) Contribution to overall identified unique phosphopeptides by each round of TiO_2 or IMAC enrichment.
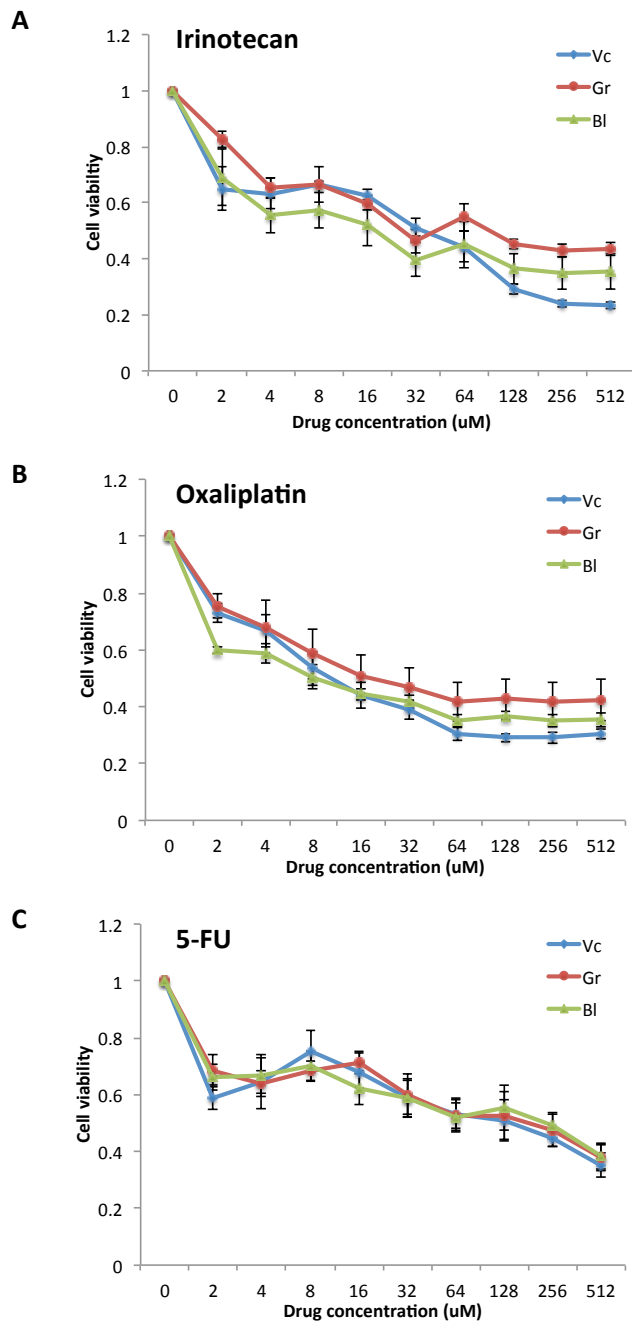
In summary, we have determined that the optimal enrichment strategy for phosphopeptides is to combine the IMAC and TiO_2 to enrich different subsets of phosphopeptides from the whole cell lysate. We are currently preparing a manuscript on these results that will shortly be submitted to the *Journal of Proteome Research*, as a follow-up to our manuscript from last year. The approach in this part will allow us to include the studies on phosphoproteomic changes caused by CDH1 knock down as well, which will further enrich our conclusions.

3. (Task 1d) Cellular responses with/without reducing CDH1 expression. (8/1/2013-9/30/2013, 2/1/2014-5/31/2014, 7/1/2014-current)

In order to find the conditions where CDH1 has clear effects on drug resistance, we treated cells with three different anti-cancer drugs including irinotecan, oxaliplatin, and 5-FU with 3D culture system. With irinotecan treatment, at lower concentration, the CDH1 knock-down cells haven't shown much resistance to irinotecan treatment, however, when the concentration reaches higher than 64 μM, both Gr and Bl cell lines that target different parts of CDH1 showed clearly higher cell viability after drug treatment compared with control cells (Vc) (**Figure 8A**). With oxaliplatin treatment, cells show similar reaction as to irinotecan treatment. At lower concentration, the CDH1 knock-down cells haven't shown much resistance to oxaliplatin treatment, however, when the concentration reaches higher than 16 μM, both Gr and Bl cell lines showed clearly higher cell viability after drug treatment compared with control cells (Vc) (**Figure 8B**). In comparison to irinotecan and oxaliplatin, CDH1 knock down cells do not show any resistance to 5-FU treatment at any concentration (**Figure 8C**).
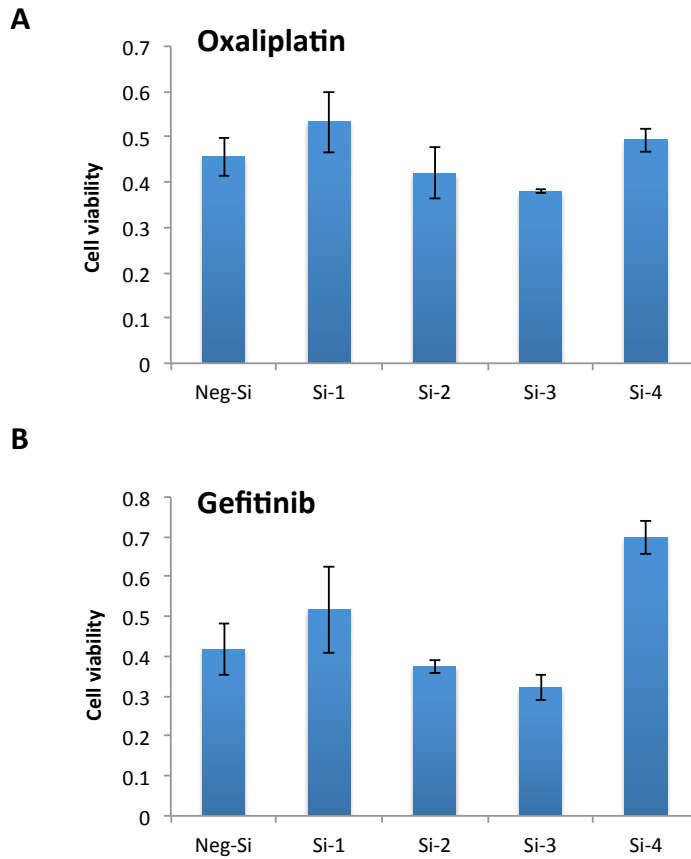
The drug resistance test with 3D systems took longer than we expected due to the optimization of test methods. We originally used agarose-coated surfaces for 3D culture. However, because the drugs can diffuse to the agarose layer that will affect the actual drug concentration, the culture system with agarose-coated surface introduced errors and was not stable between different batches of tests. On the other hand, the agarose-coated surface cannot be directly used for cell viability assays and the 3D structures together with the cells that detached from the 3D structures need to be transferred to new plates for cell viability assays. This complication will introduce even more errors to the test. After generating a substantial amount of data with the agarose-coated culture system without being able to identify any patterns of reaction to drug treatment, we concluded that the agarose-coated culture system is not a very suitable system for testing cell reactions to drug treatment. We then tried the ECM coated surface. On the ECM coated surface, the cells also automatically grow into 3D spheroids, however, it is hard to control that each well only has a single spheroid. And also, even though the ECM surface is a thinner layer, it still has variability in drug diffusion. We finally switched to Ultra-Low Attachment (ULA) round bottom plates, which perfectly solved all the problems in our tests. These plates do not need extra coating with agarose, and can be directly used for cell viability assays without transferring cells into other plates. With the ULA plates, we finally got the above results shown in **Figure 8**.

Figure 8

Fig 8. Cell viability after (A) irinotecan, (B) oxaliplatin and (C) 5-FU treatment. Blue line indicates control cells (Vc), red (Gr) and green (Bl) lines indicate CDH1 knock down cells.

To further confirm the effects of CDH1 knock-down on drug resistance, we tried other 4 different siRNAs that targets CDH1. And we tested 2 anti-cancer drugs including oxaliplatin and gefitinib. As shown in **Figure 9**, siRNA-1 and siRNA-4 clearly show higher cell viability after drug treatment, which further confirmed that knock-down of CDH1 will help cancer cells acquire drug resistance.
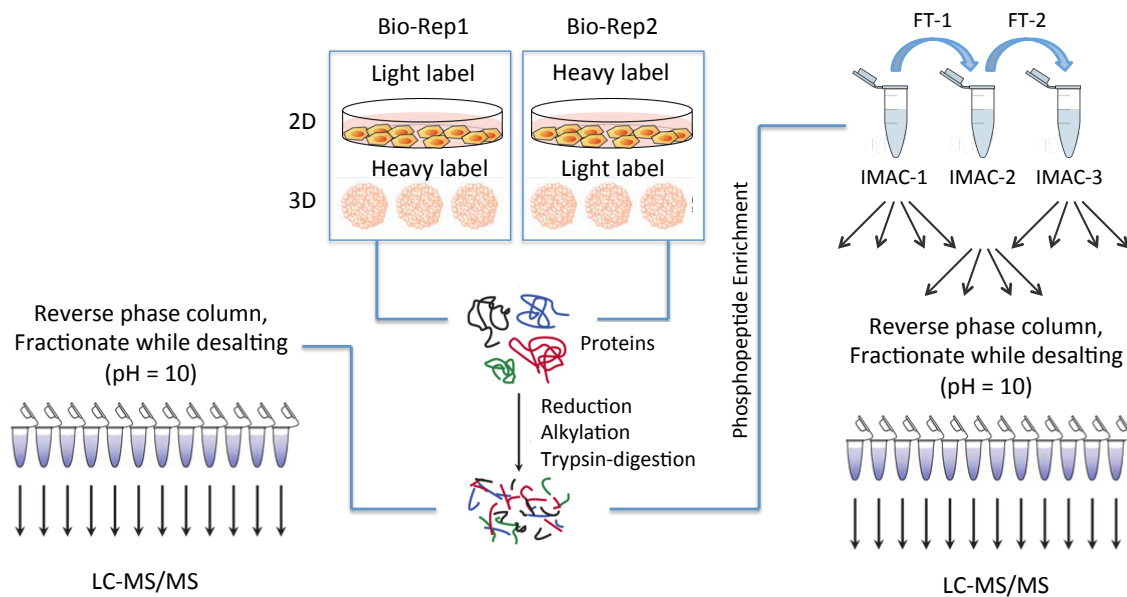
Figure 9

Fig 9. Cell viability after (A) oxaliplatin and (B) gifitinib treatment. Neg-si indicates cells transfected with siRNA that has non-specific targets. Si-1, Si-2, Si-3, and Si-4 indicate cells transfected with different siRNA sequences that targets distinct parts of CDH1 to induce CDH1 knock down.

4. (Task 2b & 2c) Collect mass spectral data for comparison of 3D-structures with or without CDH1 knockdown induction after drug treatment with the condition confirmed in 1d, and data analysis with MASCOT search engine to identify affected protein. (2/1/2014-6/30/2014)

Currently we are still in the step of sample preparation and mass spectral data collection stage for the analysis of pathways related to CDH1 knockdown caused drug resistance. While optimizing the drug treatment system and conditions, we analyzed the differences between 2D and 3D culture system as an extension of the current project. The experimental procedures are shown in **Figure 10**. 2D and 3D cultured cells were differently labeled with "light" or "heavy" amino acids and lysed to extract proteins and then mixed together. After alkylation and trypsin digestion, the peptides were divided into 2 parts. One part was fractionated with high pH reverse phase column for proteomic analysis. The other part was treated with IMAC to enrich phosphopeptides, and the enriched phosphopeptides were further fractionated with high pH reverse phase column for phosphoproteomic analysis (**Figure 10**).
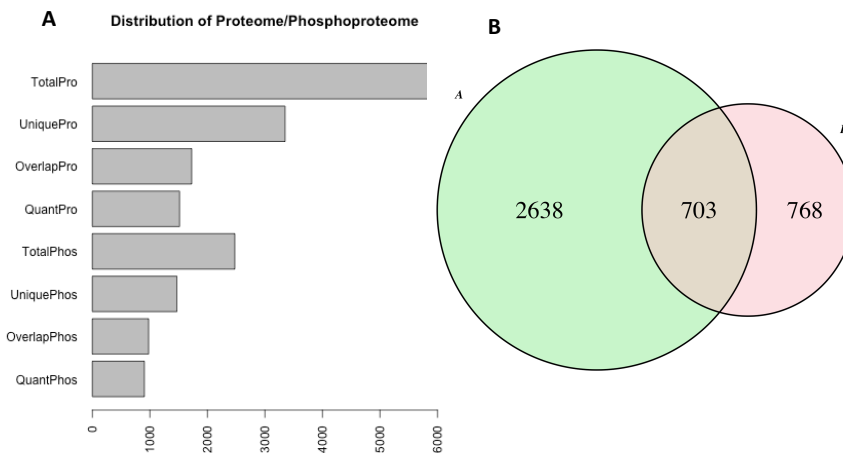
Figure 10

Fig 10. Flow chart of experiment methods for proteomic and phosphoproteomic analysis to compare 2D and 3D cultured cells.

The results are summarized in **Figure 11**. We identified a total of 5834 protein groups, including 2478 phosphoprotein groups and 8555 phosphopeptides. Among these identified results, 3348 were unique protein groups, 1471 were unique phosphoprotein groups, and 6488 were unique phosphopeptides. 2468 unique protein groups, 979 unique phosphoprotein groups, and 2069 unique phosphopeptides were identified in both biological replicates (**Figure 11A**). Of all these identifications, 703 protein groups were identified in both non-phosphorylated and phosphorylated states (**Figure 11B**).
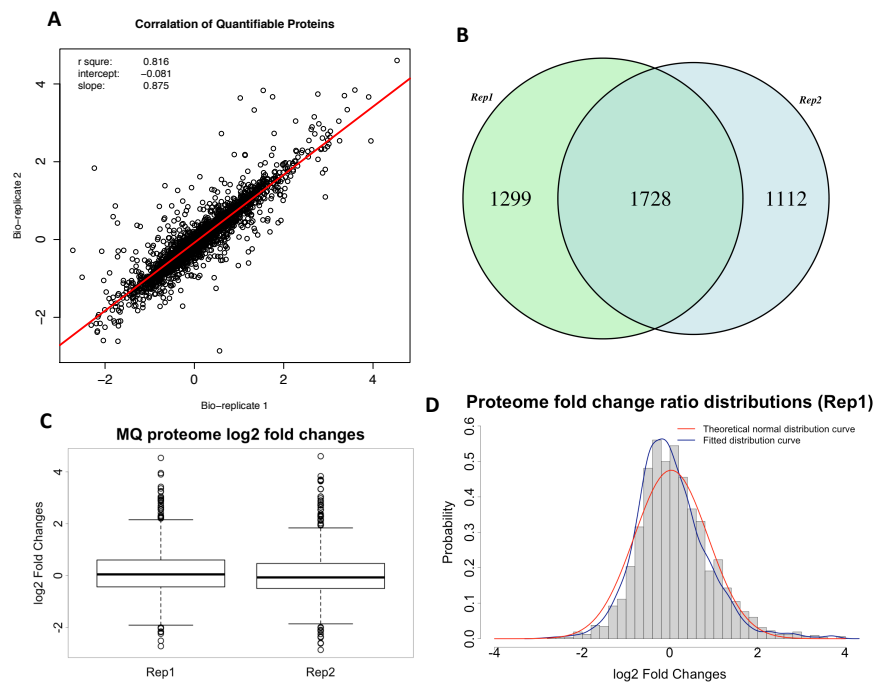
Figure 11

Fig 11. Summarization of identified proteomic and phosphoproteomic data. (A) Distribution of total protein groups, unique protein groups, phosphoprotein groups, and unique phosphoprotein groups. (B) Overlap between unique protein groups and phosphoprotein groups.

The data quality was further confirmed in **Figure 12** and **Figure 13**. **Figure 12** shows the data quality of the mass spectrometric proteomic analysis. The correlation of biological replicate 1 and biological replicate 2 showed a linear trend and the R squared value is 0.816, indicating high correlation between the 2 biological replicates (**Figure 12A**). The overlap between biological replicate 1 and biological replicate 2 shows 1728 quantifiable protein groups (**Figure 12B**), and most of the quantifiable protein groups did not show much change in the 2D or 3D cultured cells (**Figure 12C & D**). We chose 2 fold as a cutoff level to determine whether a protein has different expression levels or not in the 2D and 3D cultured cells.
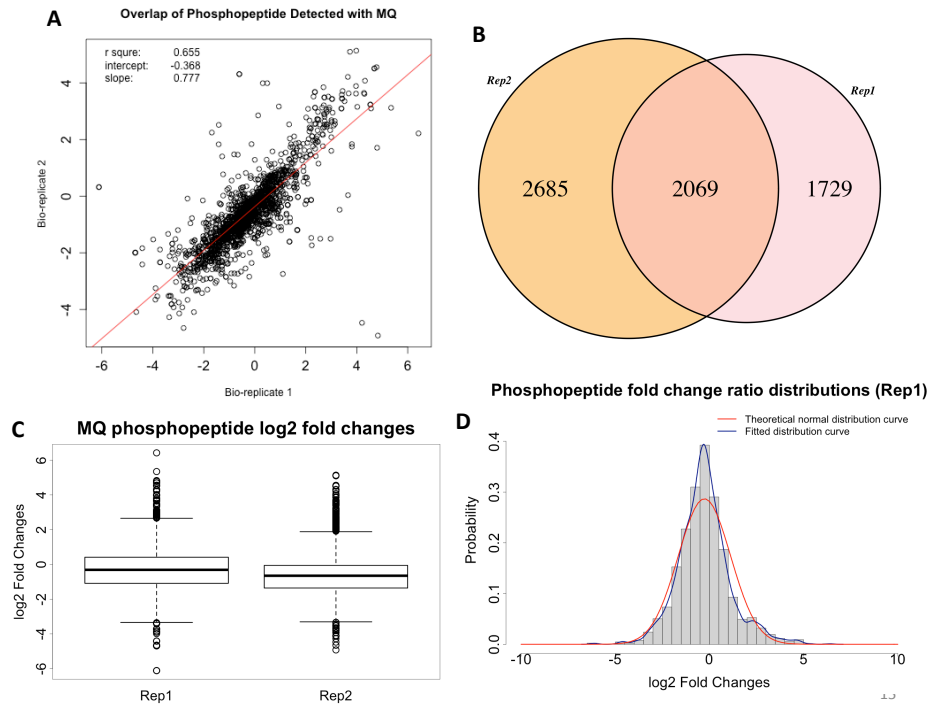
The data quality of phosphoproteomic analysis is shown in **Figure 13**. Similar to proteomic analysis, the correlation of biological replicate 1 and biological replicate 2

showed a linear trend and the R squared value is 0.655 for phosphopeptides, indicating some correlation between the 2 biological replicates (**Figure 13A**). The overlap between biological replicate 1 and biological replicate 2 shows 2069 quantifiable phosphopeptides (**Figure 13B**), and most of the quantifiable phosphopeptides didn't show many changes in the 2D or 3D cultured cells (**Figure 13C & D**). We chose 2 fold as the cutoff level to determine whether a phosphopeptide has different phosphorylation level or not in 2D and 3D cultured cells.
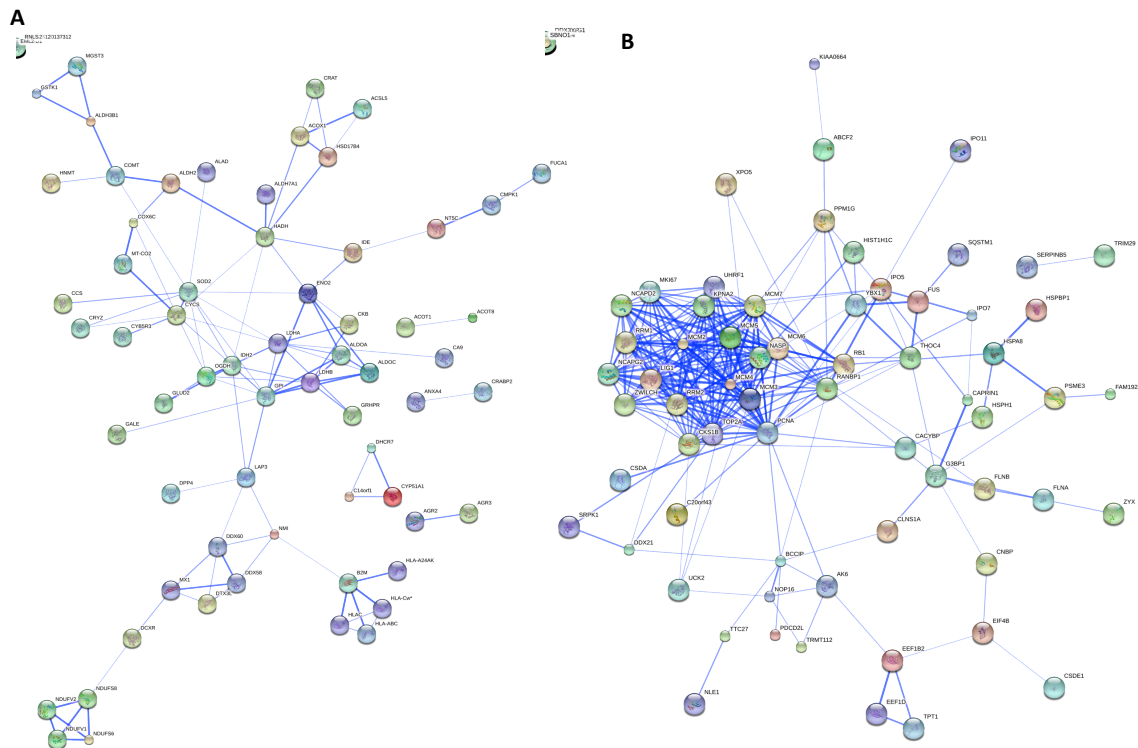
Figure 12

Fig 12. Data quality of protein groups. (A) Correlation between 2 biological replicates. (B) Overlap between 2 biological replicates. (C, D) Fold change distributions of quantifiable protein groups.

Figure 13

Fig 13. Data quality of phosphoprotein groups. (A) Correlation between 2 biological replicates. (B) Overlap between 2 biological replicates. (C, D) Fold change distributions of quantifiable phosphoprotein groups.

From the above analysis, we identified 225 protein groups and 136 phosphopeptides (representing 78 phosphoproteins) that are up-regulated in 3D cultured cells, and 116 protein groups and 422 phosphopeptides (representing 245 phosphoproteins) that are down-regulated in 3D culture cells. The network analysis shows that many of the up-regulated proteins are interconnected (**Figure 14A**), and many of the down-regulated proteins are interconnected as well (**Figure 14B**). More detailed analysis is still in process.

Figure 14

Fig 14. Network analysis of up- or down-regulated protein groups. (A) Interactions among proteins that are up-regulated in 3D cultured cells. (B) Interactions among proteins that are down-regulated in 3D cultured cells.

CONCLUSION

In the second year of research, we successfully optimized the SILAC methods and phosphoproteomic analysis methods. The optimized method has increased the phosphopeptide identification for 2 folds. We also optimized the system for testing drug effects. Four different drugs including irinotecan, oxaliplatin, 5-FU, and gefitinib were tested with CDH1 knock down cells for drug resistance effects. Cells with down regulated CDH1 levels show resistance to all drugs at high concentration except 5-FU. The mass spectrum data for drug resistance pathways are under collection and investigation. We also analyzed the proteomic and phosphoproteomic differences between 2D and 3D cultured cells.

In conclusion, during the second year, we accomplished most of the work we proposed in our original proposal, and finished the tasks that got delayed during the first

year. The second year's research is a good extension of the first year research, and provided us the foundation for our future work.

IMPACT

1. Successfully optimized SILAC conditions.

2. Successfully optimized methods for phosphoproteomic analysis.

3. Successfully confirmed the drug concentrations that CDH1 knock down show clear drug resistance effects.

4. Generated data and successfully analyzed the differences between 2D and 3D cultured colorectal cancer cells.

5. Successfully started sample preparation and mass spectral data collection steps for the analysis of pathways related to CDH1 knockdown caused drug resistance.

CHANGES/PROBLEMS

The main problem we encountered during the second year of the research is determining the drug treatment conditions that CDH1 knock-down cells show drug resistance. We originally used agarose-coated surfaces for 3D culture. However, because the drugs can diffuse to the agarose layer that will affect the actual drug concentration, the culture system with agarose-coated surface introduced errors and was not stable between different batches of tests. On the other hand, the agarose-coated surface cannot be directly used for cell viability assays and the 3D structures together with the cells that detached from the 3D structures need to be transferred to new plates for cell viability assays. This complication will introduce even more errors to the test. After generating a substantial amount of data with the agarose-coated culture system without being able to identify any patterns of reaction to drug treatment, we concluded that the agarose-coated culture system is not a very suitable system for testing cell reactions to drug treatment. We then tried the ECM coated surface. On the ECM coated surface, the cells also automatically grow into 3D spheroids, however, it is hard to control that each well only has a single spheroid. And also, even though the ECM surface is a thinner layer, it still has variability in drug diffusion. We finally switched to Ultra-Low Attachment (ULA) round bottom plates, which perfectly solved all the problems in our tests. These plates do not need extra coating with agarose, and can be directly used for cell viability assays

without transferring cells into other plates. With the ULA plates, we finally solved the problems and successfully determined the drug treatment conditions. However, this caused some delay of the second year research and the collection of proteomic and phosphoproteomic data is still in process.

PRODUCTS

Manuscripts:

Yue XS, Hummon AB. Combining of IMAC and TiO_2 enrichment methods to increase phosphoproteomic identifications, manuscript in preparation.

Yue XS, Hummon AB. Proteomic and phosphoproteomic analysis of differential protein expression and phosphorylation patterns in 2D and 3D cultured colorectal cancer cells, manuscript in preparation.

Presentations:

Yue XS, Hummon AB. Proteomic and phosphoproteomic analysis of differential protein expression and phosphorylation patterns in 2D and 3D cultured colorectal cancer cells (American Society for Mass Spectrometry Annual Meeting; Baltimore, MD; June, 2014)

Yue XS, Hummon AB. Modeling of EMT process in 3D cultures and proteomic analysis of differential protein expression in EMT related drug resistance in colorectal cancer cells (American Association for Cancer Research Special Conference; June, 2014).

Yue XS, Hummon AB. Proteomic and phosphoproteomic analysis of differential protein expression and phosphorylation patterns in 2D and 3D cultured colorectal cancer cells (Harper Day Symposium; Notre Dame IN, April, 2014)

PARTICIPANTS & OTHER COLLABORATING ORGANIZATIONS

Unchanged

SPECIAL REPORTING REQUIREMENTS

Not applicable.

APPENDICES None

REFERENCES

[1] Kang Y, MassaguéJ. Epithelial-mesenchymal transitions: twist in development and metastasis. Cell. 2004; 118(3):277-9.

[2] Yilmaz M, Christofori G. EMT, the cytoskeleton, and cancer cell invasion. Cancer Metastasis Rev. 2009; 28(1-2):15-33.

[3] Lu MH, Huang CC, Pan MR, Chen HH, Hung WC. Prospero homeobox 1 promotes epithelial-mesenchymal transition in colon cancer cells by inhibiting E-cadherin via miR-9. Clin Cancer Res. 2012; 18(23):6416-25.

[4] McConkey DJ, Choi W, Marquis L, Martin F, Williams MB, Shah J, Svatek R, Das A, Adam L, Kamat A, Siefker-Radtke A, Dinney C. Role of epithelial-to-mesenchymal transition (EMT) in drug sensitivity and metastasis in bladder cancer. Cancer Metastasis Rev. 2009; 28(3-4):335-44.

[5] Voulgari A, Pintzas A. Epithelial-mesenchymal transition in cancer metastasis: mechanisms, markers and strategies to overcome drug resistance in the clinic. Biochim Biophys Acta. 2009; 1796(2):75-90.

[6] Frisch SM, Schaller M, Cieply B. Mechanisms that link the oncogenic epithelial-mesenchymal transition to suppression of anoikis. J Cell Sci. 2013; 126(Pt 1):21-9.

[7] Ilya Serebriiskii, Remedios Castelló-Cros, Acacia Lamb, Erica A. Golemis, Edna Cukierman. Fibroblast-derived 3D matrix differentially regulates the growth and drug-responsiveness of human cancer cells. Matrix Biol. 2008; 27(6): 573–585.

[8] Baharvand H, Hashemi SM, Kazemi Ashtiani S, Farrokhi A. Differentiation of human embryonic stem cells into hepatocytes in 2D and 3D culture systems in vitro. Int J Dev Biol. 2006; 50(7):645-52.

[9] Han J. and Chang H., et al. Multiscale iterative voting for differential analysis of stress response for 2D and 3D cell culture models. J Microsc 2011; 241(3): 315-26.

[10] Mishra, DK. and Sakamoto JH, et al. Human lung cancer cells grown in an ex vivo 3D lung model produce matrix metalloproteinases not produced in 2D culture. PLoS One 2012; 7(9): e45308.

[11] Chitcholtan K. and Asselin E., et al. Differences in growth properties of endometrial cancer in three dimensional (3D) culture and 2D cell monolayer. Exp Cell Res. 2013; 319(1): 75-87.

[12] Taus T, Kocher T, Pichler P, Paschke C, Schmidt A, Henrich C, Mechtler K (2011). Universal and confident phosphorylation site localization using phosphoRS. J Proteome Res, 10(12):5354-5362